THE JOURNAL OF PHYSICAL CHEMISTRY B

ARTICLE

pubs.acs.org/JPCB

Hydrophobic Transition in Porous Amorphous Silica

Bertrand Siboulet,[*,†] Benoît Coasne,[‡] Jean-François Dufrêche,[*,§] and Pierre Turq[§,∥]

[†]CEA, DEN, ICSM, Marcoule, F-30207 Bagnols-sur-Cèze, France

[‡]Institut Charles Gerhardt Montpellier, ENSCM, Université Montpellier 2 and CNRS (UMR 5253), 8 rue Ecole Normale, F-34296 Montpellier, France

[§]Institut de Chimie Séparative de Marcoule ICSM, UMR 5257 CEA - CNRS - ENSCM - Université Montpellier 2, Bâtiment 426, F-30207 Bagnols-sur-Cèze, France

[∥]Université Pierre et Marie Curie Paris VI, UMR 7195, PECSA, F-75005 Paris, France

ABSTRACT: Realistic models of amorphous silica surfaces with different silanol densities are built using Monte Carlo annealing. Water−silica interfaces are characterized by their energy interaction maps, adsorption isotherms, self-diffusion coefficients, and Poiseuille flows. A hydrophilic to hydrophobic transition appears as the surface becomes purely siliceous. These results imply significant consequences for the description of surfaces. First, realistic models are required for amorphous silica interfaces. Second, experimental amorphous silica hydrophilicity is attributed to charged or uncharged defects, and not to amorphousness. In addition, autoirradiation in nuclear waste glass releases hydrogen atoms from silanol groups and can induce such a transition.

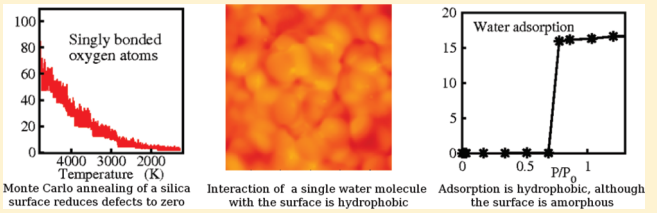

Monte Carlo annealing of a silica surface reduces defects to zero

Interaction of a single water molecule with the surface is hydrophobic

Adsorption is hydrophobic, although the surface is amorphous

INTRODUCTION

Porous silicas are of both fundamental and practical interest, as they exhibit a large specific surface and a porosity network that can be precisely tuned (pore size and morphology). Moreover, their surface can be functionalized with a variety of molecules and groups. As a result, porous silicas find important industrial applications in catalysis, phase separation, storage and separation of radionuclides, nanofiltration, drug delivery, medical diagnosis, etc.[1] An important parameter, which controls most of these processes, is the silanol surface density. Such polar groups are hydrophilic and control the adsorbate/surface interaction strength and the adsorbate mobility,[2] the solvent structure depending strongly on this interaction.[3] The silanol density can be tuned by different procedures such as heating or irradiating the silica sample. In nuclear glass, autoirradiation has a potential impact on silanol density. Indeed, it has been established that the observed release of hydrogen from irradiated silicates results from the radio-induced emission of protons from the surface silanol groups.[4] Understanding the role played by these groups in the hydrophilic or hydrophobic nature of silica requires estimating the thermodynamics and dynamics of adsorbed or confined water in realistic models[5−7]

In this Article, we begin by building a realistic model of amorphous silica surfaces, using Monte Carlo (MC) simulations combined with a simulated annealing technique. Such an amorphous model, which is obtained through a physical annealing procedure, differs from conventional models obtained by a random or simple thermalization of a crystalline silica surface. A slit pore is then built by considering two of these surfaces at a distance of H = 2 nm from each other. We use this setup to investigate the relationship between the silanol surface density and the degree of hydrophilicity/hydrophobicity, by measuring the thermodynamics (surface energy maps and adsorption) and dynamics (self-diffusion and hydrodynamic flow) of water in a realistic model of porous silica.

Building Realistic Amorphous Surfaces. *Monte Carlo Simulations on Pure Silica.* Canonical ensemble (NVT) MC simulations, combined with a simulated annealing technique, are performed to build a model of amorphous silica surfaces using the BKS potential.[8] This force-field was chosen because it accurately describes the structure and vibrational spectra of bulk silica.[9] The initial configuration consists of a square slab of pure silica, 1.2 nm thick with a lateral size of 2.852 nm, with a periodically replicated cubic simulation box of size 2.852 nm. Annealing is simulated from 5000 to 1300 K. At each temperature, a series of 10 runs, of 5×10^5 MC trials each, is performed. The old temperature T_{old} is then decreased to obtain the new temperature $T_{new} = 0.99T_{old}$. Among typical defects encountered in amorphous silica surfaces, oxygen atoms with a dangling bond (a Si−O pair is bonded if the distance is below 0.2 nm) are the most hydrophilic. Figure 1 shows that the number of oxygen dangling bonds N_{db} in the amorphous silica slit decreases upon annealing, as these defects, which correspond to high energy states due to the creation of long-range dipolar fields, are slowly healed. By fitting the results shown in Figure 1 using a Van't Hoff law, the enthalpy of formation of these defects was found to be

Received: April 6, 2011
Revised: May 13, 2011
Published: June 01, 2011

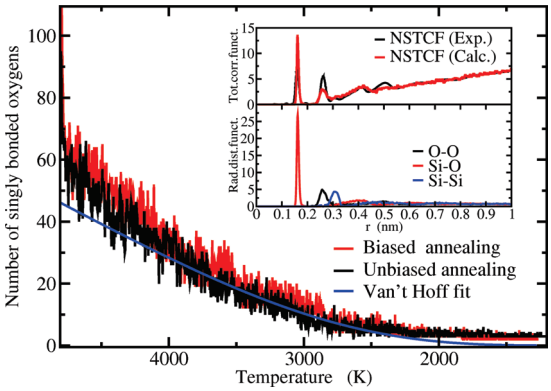

Figure 1. Number of oxygen dangling bonds N_{db} upon annealing for a silica surface: (black) unbiased annealing, (red) biased annealing in which a run is retained if N_{db} is lower than in the previous run. The blue line is a fit by a Van't Hoff law. In the inset are shown the radial distribution functions and the neutron diffraction analysis.

close to 100 kJ·mol^{-1}. After annealing, N_{db} = 3 in the final structure of the amorphous silica surface. These three defects are very unlikely at low temperature because of their energy cost. In a more rigorous annealing simulation, with a slower temperature decrease, they would probably disappear. Thus, biased simulations are performed to obtain defect free surfaces: at the end of each MC run, the final configuration is retained only if N_{db} is lower than in the previous run. As shown in Figure 1, biased simulations are more efficient at reducing the number of defects, as N_{db} = 2 in the final biased structure. The two defects, being on the same side, leave a defect free side which is used throughout this work. The inset in Figure 1 shows the partial radial distribution functions $g_{OO}(r)$, $g_{SiO}(r)$, and $g_{SiSi}(r)$ for this structure. We also show the neutron scattering total correlation function (NSTCF) given by $h(r) = 4\pi(4b_O^2 g_{OO}(r) + 4b_O b_{Si} g_{SiO} + b_{Si}^2 g_{SiSi}(r))$, where the scattering lengths are b_O = 5.805 fm and b_{Si} = 4.151 fm. The simulated NSTCF, which has been divided by a factor of $(1 - (r/2l))$ to correct for the finite width (l) of the silica slab, corresponds to the experimental data for bulk silica.[10] This result shows that, after annealing, the amorphous silica slit is locally close to bulk silica with a weakly perturbed tetrahedral network. A similar biasing technique has been used in a molecular dynamics (MD) study.[11]

Addition of Silanols on Surfaces. More hydrophilic silica surfaces are obtained when different numbers of silanol groups are added on the surface obtained using the procedure above. To do that, surface oxygen atoms are homogeneously selected and replaced by pairs of OH groups. The new structure is then allowed to relax in the course of a MD run. As in the MC simulations, the BKS potential[8] is used, while the interaction between the H and O atoms of the same silanol group is described through a Morse potential.[12] A purely repulsive Buckingham potential between nonbonded O−H pairs is initially included.[13] This relaxation method (r1) is discarded (see below). In a second try, an additional repulsive r^{-6} term is added to avoid excessive hydrogen bonding between OH groups (relaxation r2), which originates in the unphysical absence of water during relaxation. Two silanolated surfaces with 3.7 and 7.1 OH nm^{-2} were prepared. They correspond to typical densities in real amorphous porous silicas.[14,15] While silanol free surfaces are encountered in crystalline materials such as zeolites,[16] they are not observed in amorphous siliceous materials (probably due to spontaneous hydroxylation of the surface in contact with water). Nevertheless, the limiting case of the silanol free silica surface can be seen as a model of irradiated silicates that tend to be deprotonated due to the radio-induced emission of protons from the surface.[4]

Table 1. *nm* Parameters for Water/Surface Interaction[a]

water species	silica species	E_0 10^{-4} Ha	r_0 a_0	n	m
Hw	O	1.810	5.724	8.25792	8.25791
Hw	Si	0.134	7.205	13.2725	6.71192
Hw	H	1.861	3.965	6.32666	6.32705
Ow	O	2.507	6.999	11.61320	7.28875
Ow	Si	0.2777	8.199	15.49670	6.58589
Ow	H	1.493	5.530	7.85993	7.85989

[a] The PN-TrAZ potential[19] cannot be input in DL_POLY but is accurately fitted by an *nm* potential.[20]

Interaction Potentials. For each surface chemistry, we build a slit pore formed by two surfaces separated by a distance of H = 2 nm. The water−silica interfaces of the three structures are first characterized by calculating the energy map for a single water molecule adsorbed on their surface. The adsorption isotherm, self-diffusion, and water transport are determined at room temperature using grand canonical Monte Carlo (GCMC) simulations and MD simulations. Water is described using the SPC/E model,[17] which reasonably reproduces the experimental diffusion coefficient[17] and viscosity[18] of bulk water (2.5 vs 2.4 × 10^9 m^2 s^{-1} and 0.729 vs 0.896 mPa·s). The PN-TrAZ potential is used to describe the water/surface interaction[19,20] with the following partial atomic charges $q_O = -1.0$, $q_{Si} = 2.0$, and q_H = 0.5. The Coulomb energy is computed using the Ewald sum with 10^3 k vectors and a real space cutoff of 1.5 nm. All interaction potentials are listed in Table 1. The non-Coulombian interaction between a water atom $k = H_w$, O_w and a surface atom j = O, Si, H is

$$U_{kj}(\vec{r}_{kj}) = \frac{E_0}{n-m}\left[m\left(\frac{r_0}{r_{jk}}\right)^n - n\left(\frac{r_0}{r_{jk}}\right)^m\right] \quad (1)$$

Surface Interaction Mapping. Figure 2 shows the energy map of a water molecule on top of these different surfaces: (a) the silanol free surface and the surfaces, (b) with 3.7 and (c) 7.1 OH nm^{-2}. The corresponding energy histograms are shown in Figure 2d. Each map represents the lowest energy along the z axis at a given position (x,y) (at each grid point, the molecule orientation is relaxed to optimize the interaction). The absolute value of the adsorption energy for the silanol free surface is always smaller than the heat of condensation of bulk water (17.7 kT), which tends to indicate the hydrophobic nature of this surface. In contrast, the surfaces with nonzero silanol densities exhibit hydrophilic regions where the interaction energy is larger than 17.7 kT.

Adsorption. *Modeling Adsorption with GCMC.* The hydrophilicity/hydrophobicity of the silica surfaces was further investigated by simulating water adsorption. The adsorption isotherm is given in GCMC simulations by the ensemble average of the number of adsorbed molecules as a function of the relative pressure of the gas reservoir P/P_0; P is obtained from the chemical potential μ according to the bulk equation of state for

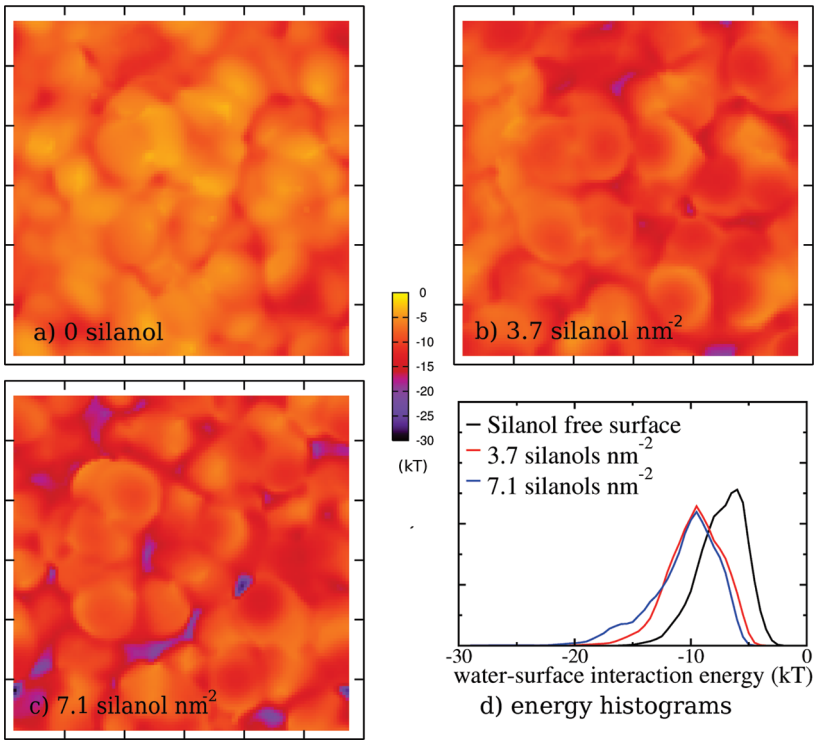

Figure 2. Energy map for a single water molecule adsorbed on top of silica surfaces: (a) silanol free surface, (b) with 3.7 OH nm^{-2}, and (c) with 7.1 OH nm^{-2}. (d) Energy histograms of the surface energy maps shown in parts a, b, and c.

an ideal gas, and $P_0 = 2900$ Pa corresponds to the saturating vapor pressure of the SPC/E model at 300 K.[21]

The water adsorption isotherms at 300 K are shown in Figure 3 for the porous silica surfaces having 0, 3.7, and 7.1 OH nm^{-2} obtained with the r2 relaxation (see above). For the surface with 7.1 OH nm^{-2}, we also show results obtained on a reference case, where OH groups rotate freely (fh). We performed this extra simulation for the following reason. Silanol protons are mobile, but this is not accounted for in our surface model, so as to reduce CPU time by approximately 100. Including proton mobility can only increase water surface interaction and eventually modify the surface hydrophilicity. It is important to check on a reference case that the impact of proton mobility is small, so that the use of r2 is valid for our purpose. We also show results when silanol is relaxed with a short-range Buckingham repulsion (r1). Comparison of the three curves shows why the relaxation r1 should be discarded in favor of r2: r2 adsorption at low pressure perfectly fits the reference fh, whereas r1 underestimates it by a factor of 2. The use of r1 is precluded for a quantitative analysis, while r2 reduces the CPU time but does not quantitatively modify the final result. For all surface chemistries, the adsorbed amount increases linearly with pressure in the adsorption regime (at low pressures) until a jump occurs due to capillary condensation of water within the pore. At a given pressure prior to capillary condensation, the adsorbed amount increases as the surface density of silanol groups increases. This result is consistent with the fact that the isosteric heat of adsorption increases with an increase in density of OH groups: Q_{st} = 23, 40, and 55 kJ·mol^{-1} for 0, 3.7, and 7.1 OH nm^{-2}. The adsorption isotherms in Figure 3 are characteristic of surfaces varying from hydrophobic to hydrophilic materials. This result, which is in fair agreement with the experimental data for various amorphous silica surfaces,[22] indicates a hydrophobic to

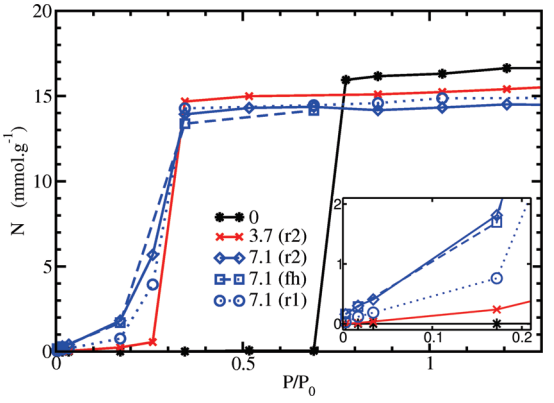

Figure 3. Water adsorption isotherms in a silica pore of width $H = 2$ nm with different surface chemistries: (black) 0, (red) 3.7, and (blue) 7.1 OH nm^{-2}. The two last blue sets are for the reference surface with 7.1 OH nm^{-2}, where the OH groups are allowed to rotate (fh, dashed), or without the intersilanol O−H extra repulsive term (r1, dotted).

hydrophilic transition between 0 and 3.7 OH nm^{-2}. Such a result corroborates the fact that capillary condensation is shifted toward lower pressures with increasing hydrophilicity.

Comparison with Experimental Data. We now discuss the validity of the method we use for building the amorphous surfaces. For this, we compare in more details our modeled adsorptions with experiments and with adsorption modeled with surfaces obtained from crystalline materials. The validity of adsorption models at low coverage depends on the accuracy of the water/surface interaction, and at higher coverage on the mesoporous network and on the water/water interaction. This is why, in order to establish the validity of our amorphous surfaces,

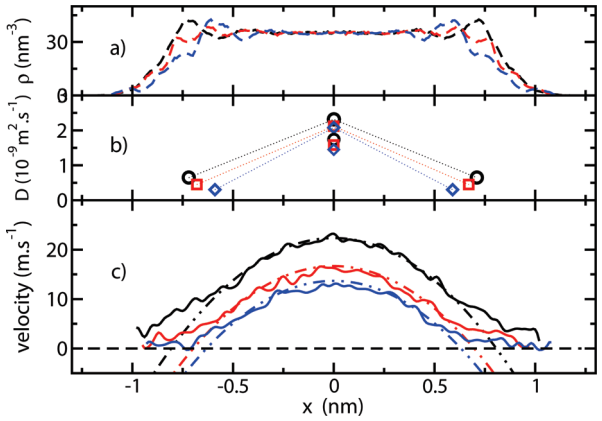

Figure 4. (a) Density, (b) diffusion coefficients, and (c) velocity profiles for water at 300 K in a silica nanopore of width H = 2 nm with different surface chemistries: (black) 0, (blue) 3.7, and (red) 7.1 OH nm^{-2}. x is the position with respect to the pore center. Total pore average diffusion coefficients are plotted at x = 0.

we should focus on low coverage values, prior to capillary condensation. We compare values at P/P_0 = 0.2, which is below condensation in all cases. In the case of a MCM-41 sample, which includes substantial hydroxylation, Takahara et al. show that adsorption starts linearly with pressure.[23] The average water thickness is 0.06 and 0.12 nm for first and second adsorption. On an other MCM-41 sample, Llewellyn et al. estimate to 1.2 OH nm^{-2} the hydroxyl surface density.[24] The surface is "relatively hydrophobic", and adsorption starts linearly with pressure. The water layer thickness is 0.12 nm at P/P_0 = 0.2. These results are in agreement with our model as we find for 0, 3.7, and 7.1 OH nm^{-2}, at similar pressure, 10^{-4}, 0.015, and 0.12 nm for the water layer thickness. On the other hand, if the surface is carved out of a crystal instead of being amorphous, one finds 0.6 nm for the same pressure and 0.2 for P/P_0 = 0. For both criteria, initial and low pressure coverage, the amorphous surface is significantly more representative. These results show that a quantitative description of adsorption on silica surfaces requires taking into account its amorphous nature. Other experimental results support the latter conclusion: for MCM-41,[25,26] FSM-16,[27] and SBA-15.[28] However, while our coverage values are consistent with experiment, they are inferior to experimental values. This is believed to be due to residual defect concentrations, especially charged defects, which increase water uptake at low pressures. The silanol free surface coverage is well below experimental values, but amorphous silica surfaces have residual defect concentration, e.g., silanols. Indeed, crystalline structures can show very hydrophobic defect free surfaces, such as zeolite, e.g., in the case of silicalite-1.[16,29,30]

Transport Properties: Diffusion and Hydrodynamics. *Diffusion Coefficients.* We also investigated the impact of the hydrophobic/hydrophilic nature of the silica surface on the dynamical properties of confined water. Starting with well equilibrated configurations obtained from GCMC simulations, we determined the self-diffusivity and transport of water confined within the pores with 0, 3.7, and 7.1 OH nm^{-2}. The same interaction potentials as those used in the GCMC runs were considered in the MD runs. The MD runs are performed in the *NVT* ensemble at 300 K using the Berendsen thermostat with a relaxation time of 0.01 ps. Trajectories are integrated using the Verlet leapfrog algorithm with a time step of 1 fs. After an equilibration time of 300 ps, data were averaged over 1 ns. Figure 4a shows the density profile of water confined within the three slit pores with different surface chemistries. As is usually observed for confined water and other fluids, the density exhibits marked oscillations that reveal the layering of the fluid in the vicinity of the surfaces. Using the mean square displacement, self-diffusion coefficients D have been determined for molecules in the pore center and inside boundary layers,[31] i.e., in contact with the silica surface (Figure 4b). On the basis of the density profiles, the boundary layers were defined as water molecules located between the first two minima in the density profile. In the pore center, D is very close to that of bulk SPC/E ($D_0 = 2.5 \times 10^{-9}$ m$^2\cdot$s^{-1}) for all surface chemistries. In contrast, D in the boundary layers is smaller than in the pore center and depends on the surface chemistry: 0.65, 0.45, and 0.30 $\times 10^{-9}$ m$^2\cdot$s^{-1} for 0, 3.7, and 7.1 OH nm^{-2}, the surface diffusion being greater for the more hydrophobic surfaces.

Poiseuille Flows. We also determine the collective dynamical properties of confined water by calculating the Poiseuille hydrodynamic flow resulting from an external force f parallel to the surfaces. In a slit geometry, the hydrodynamic flow is given by the Navier−Stokes equation:

$$v(x) = -\frac{f}{2\eta}x^2 + v_{\max} \qquad (2)$$

where x is the position relative to the pore center, η the viscosity, and $v_{\max}$ the maximal velocity which depends on the hydrodynamic boundary conditions at the surface. The velocity profile obtained for each silica surface in Figure 4c is fitted using eq 2 in which we impose the viscosity of the SPC/E model. The fit in the pore center region ($|x| \leq 0.5$ nm) leads to $v_{\max}$ = 22.5, 17, and 14 m$\cdot$s^{-1} for the silica surfaces with 0, 3.7, and 7.1 OH nm^{-2}. Hydroxylation of the silica divides the flow by a factor of 1.6 or 2.2 when compared to the silanol free surface. Such a decrease of the flow with increasing silanol densities is due to the change in the velocity of the water molecules in the boundary layers. The latter become mobile in the case of the silanol free surface so that hydrophobic slippage appears at the surface. This can be quantified by estimating the slip length b at the hydrodynamic interface, which is defined as $dv/dx = v/b$.[32,33] When the latter is defined by the position for which the molecular hydrodynamic profile departs from the Navier−Stokes prediction, we approximately estimate b = 0.3 nm, b = 0.1 nm, and b = 0 nm for increasing silanol density. These values, which are consistent with the small slip lengths reported for weakly hydrophobic surfaces,[34] show that slippage at the pore surface becomes negligible for large porosities. Nevertheless, such slip lengths are large enough to induce important effects on the Darcy flows for nanopores, since they strongly enhance the Poiseuille flow. This also impacts separation processes, since it reduces the time the solution is in contact with the surface, and reduces the retention ability of the radionuclide. Slipping effects are even more important on electrokinetic phenomena: in the case of electro-osmosis, with such slip lengths, a factor of 10 is expected in our case at low salt concentrations.[32,35−37]

CONCLUSION

In summary, the realistic model of amorphous silica surfaces reported in this Article provides the main ingredients to understand the link between the surface chemistry of materials and their affinity for water. The thermodynamics and dynamics of

water confined in the materials with various surface chemistries show a hydrophobic to hydrophilic transition as the silanol density increases. A consistent picture of the hydrophobicity and hydrophilicity of siliceous materials emerges: silanol free surfaces are hydrophobic, and the hydrophilicity of real amorphous silica is due to its defects and not to its amorphous nature. Amorphous surfaces with non-negligible silanol densities are hydrophilic, which is in agreement with experimental data.

The surface diffusion is multiplied by a factor of 2.2 from highly hydroxylated to silanol free surfaces. Slippage appears in the case of hydrophobic surfaces, and this can lead to dramatic enhancement of hydrodynamic flows, especially in the case of electrokinetic phenomena. Such differences could be evidenced in the case of irradiated glasses by experimental techniques based on electrokinetic phenomena or dielectric spectroscopy. The results above, which help to shed light on the complex concepts of hydrophobicity and hydrophilicity, have important implications in the fields involving confined or vicinal water.

Comparison with adsorption experiments shows that a realistic description of amorphous silica surfaces is crucial to reproduce experimental data. In this Article, we report a straightforward method based on the Monte Carlo scheme and molecular dynamics simulation to produce such realistic models. The latter are required not only for adsorption studies but also for molecular dynamics studies or for any study involving water in contact with any amorphous surface.

AUTHOR INFORMATION

Corresponding Author

*E-mail: bertrand.siboulet@cea.fr (B.S.); jean-francois.dufreche@univ-montp2.fr (J.-F.D.).

ACKNOWLEDGMENT

The authors are particularly grateful to Thomas Zemb and Agnès Grandjean for fruitful discussions.

REFERENCES

(1) Davis, M. Ordered porous materials for emerging applications. *Nature* **2002**, *417*, 813–821.

(2) Hautman, J.; Klein, M. Microscopic Wetting Phenomena. *Phys. Rev. Lett.* **1991**, *67*, 1763–1766.

(3) Thompson, H.; Soper, A.; Ricci, M.; Bruni, F.; Skipper, N. The three-dimensional structure of water confined in nanoporous vycor glass. *J. Phys. Chem. B* **2007**, *111*, 5610–5620.

(4) Brunet, F.; Charpentier, T.; Caer, S. L.; Renault, J. Solid-state NMR characterization of a controlled-pore glass and of the effects of electron irradiation. *Solid State Nucl. Magn. Reson.* **2008**, *33*, 1–11.

(5) Cruz-Chu, E.; Aksimentiev, A.; Schulten, K. Water-silica force field for simulating nanodevices. *J. Phys. Chem. B* **2006**, *110*, 21497–21508.

(6) Coasne, B.; Hung, F.; Pellenq, R.; Siperstein, F. R.; Gubbins, K. E. Adsorption of sample gases in MCM-41 materials: The role of surface roughness. *Langmuir* **2006**, *22*, 194–202.

(7) Gelb, L. D.; Gubbins, K. E. Characterization of porous glasses: Simulation models, adsorption isotherms, and the Brunauer-Emmett-Teller analysis method. *Langmuir* **1998**, *14*, 2097–2111.

(8) Vanbeest, B.; Kramer, G.; Vansanten, R. Force-Fields for Silicas and Aluminophosphates Based on Ab Initio Calculations. *Phys. Rev. Lett.* **1990**, *64*, 1955–1958.

(9) Wilson, M.; Madden, P.; Hemmati, M.; Angell, C. Polarization effects, network dynamics, and the infrared spectrum of amorphous SiO2. *Phys. Rev. Lett.* **1996**, *77*, 4023–4026.

(10) Grimley, D.; Wright, A.; Sinclair, R. Neutron-Scattering from Vitreous Silica IV. Time-of-Flight Diffraction. *J. Non-Cryst. Solids* **1990**, *119*, 49–64.

(11) Bakaev, V.; Steele, W. On the computer simulation of a hydrophobic vitreous silica surface. *J. Chem. Phys.* **1999**, *111*, 9803–9812.

(12) Greathouse, J.; Durkin, J.; Larentzos, J.; Cygan, R. Implementation of a Morse potential to model hydroxyl behavior in phyllosilicates. *J. Chem. Phys.* **2009**, *130*, 134713–134719.

(13) Schroder, K.; Sauer, J. Potential functions for silica and zeolite catalysts based on ab initio calculations. 3. A shell model ion pair potential for silica and aluminosilicates. *J. Phys. Chem.* **1996**, *100*, 11043–11049.

(14) Zhao, X.; Lu, G.; Whittaker, A.; Millar, G.; Zhu, H. Comprehensive study of surface chemistry of MCM-41 using Si-29 CP/MAS NMR, FTIR, pyridine-TPD, and TGA. *J. Phys. Chem. B* **1997**, *101*, 6525–6531.

(15) Zhuravlev, L. Concentration of Hydroxyl-Groups on the Surface of Amorphous Silicas. *Langmuir* **1987**, *3*, 316–318.

(16) Desbiens, N.; Boutin, A.; Demachy, I. Water condensation in hydrophobic silicalite-1 zeolite: A molecular simulation study. *J. Phys. Chem. B* **2005**, *109*, 24071–24076.

(17) Berendsen, H.; Grigera, J.; Straatsma, T. The Missing Term in Effective Pair Potentials. *J. Phys. Chem.* **1987**, *91*, 6269–6271.

(18) Gonzalez, M.; Abascal, J. The shear viscosity of rigid water models. *J. Chem. Phys.* **2010**, *132*, 096101–096102.

(19) Puibasset, J.; Pellenq, R. Grand canonical Monte Carlo simulation study of water structure on hydrophilic mesoporous and plane silica substrates. *J. Chem. Phys.* **2003**, *119*, 9226–9232.

(20) Bonnaud, P.; Coasne, B.; Pellenq, R. Molecular simulation of water confined in nanoporous silica. *J. Phys.: Condens. Matter* **2010**, *22*, 284110–284124.

(21) Guissani, Y.; Guillot, B. A Computer-Simulation Study of the Liquid-Vapor Coexistence Curve of Water. *J. Chem. Phys.* **1993**, *98*, 8221–8235.

(22) Ng, E.; Mintova, S. Nanoporous materials with enhanced hydrophilicity and high water sorption capacity. *Microporous Mesoporous Mater.* **2008**, *114*, 1–26.

(23) Takahara, S.; Nakano, M.; Kittaka, S.; Kuroda, Y. Neutron scattering study on dynamics of water molecules in MCM-41. *J. Phys. Chem. B* **1999**, *103*, 5814–5819.

(24) Llewellyn, P.; Schuth, F.; Grillet, Y.; Rouquerol, F.; Rouquerol, J.; Unger, K. Water Sorption on Mesoporous Aluminosilicate MCM-41. *Langmuir* **1995**, *11*, 574–577.

(25) Chen, C.; Li, H.; Davis, M. Studies on mesoporous materials: I. Synthesis and characterization of MCM-41. *Microporous Mater.* **1993**, *2*, 17–26.

(26) Naono, H.; Hakuman, M.; Tanaka, S.; Tamura, N.; Nakai, K. Porous texture and surface character of dehydroxylated and rehydroxylated MCM-41 mesoporous silicas - Analysis of adsorption isotherms of nitrogen gas and water vapor. *J. Colloid Interface Sci.* **2000**, *225*, 411–420.

(27) Inagaki, S.; Fukushima, Y.; Kuroda, K.; Kuroda, K. Adsorption isotherm of water vapor and its large hysteresis on highly ordered mesoporous silica. *J. Colloid Interface Sci.* **1996**, *180*, 623–624.

(28) Morishige, K.; Iwasaki, H. X-ray Study of Freezing and Melting of Water Confined within SBA-15. *Langmuir* **2003**, *19*, 2808–2811.

(29) Desbiens, N.; Demachy, I.; Fuchs, A.; Kirsch-Rodeschini, H.; Soulard, M.; Patarin, J. Water condensation in hydrophobic nanopores. *Angew. Chem., Int. Ed.* **2005**, *44*, 5310–5313.

(30) Cailliez, F.; Trzpit, M.; Soulard, M.; Demachy, I.; Boutin, A.; Patarin, J.; Fuchs, A. Thermodynamics of water intrusion in nanoporous hydrophobic solids. *Phys. Chem. Chem. Phys.* **2008**, *10*, 4817–4826.

(31) Schoen, M.; Cushman, J.; Diestler, D.; Rhykerd, C. Fluids in micropores. II. Self-diffusion in a simple classical fluid in a slit pore. *J. Chem. Phys.* **1988**, *88*, 1394–1406.

(32) Marry, V.; Dufreche, J.; Jardat, M.; Turq, P. Equilibrium and electrokinetic phenomena in charged porous media from microscopic and mesoscopic models: electro-osmosis in montmorillonite. *Mol. Phys.* **2003**, *101*, 3111–3119.

(33) Joly, L.; Ybert, C.; Trizac, E.; Bocquet, L. Hydrodynamics within the electric double layer on slipping surfaces. *Phys. Rev. Lett.* **2004**, *93*, 257805–257808.

(34) Huang, D.; Cottin-Bizonne, C.; Ybert, C.; Bocquet, L. Massive amplification of surface-induced transport at superhydrophobic surfaces. *Phys. Rev. Lett.* **2008**, *101*, 064503–064507.

(35) Ajdari, A.; Bocquet, L. Giant amplification of interfacially driven transport by hydrodynamic slip: Diffusio-osmosis and beyond. *Phys. Rev. Lett.* **2006**, *96*, 186102–186105.

(36) Bocquet, L.; Barrat, J. Flow boundary conditions from nano- to micro-scales. *Soft Matter* **2007**, *3*, 685–693.

(37) Dufreche, J.; Marry, V.; Malikova, N.; Turq, P. Molecular hydrodynamics for electro-osmosis in clays: from Kubo to Smoluchowski. *J. Mol. Liq.* **2005**, *118*, 145–153.